AIAA JOURNAL
Vol. 42, No. 1, January 2004

Quadratic Stress Failure Constraints for Structures Under Combined Steady and Random Excitation

Frode Engelsen*
The Boeing Company, Seattle, Washington 98124
and
Eli Livne†
University of Washington, Seattle, Washington 98195-2400

Constraint functions are formulated and their analytical sensitivities are derived for multiaxial states of stress arising in actively controlled airplane structures from combined maneuver loads and random gust responses. The stress failure criteria of von Mises for isotropic materials and Tsai–Wu for composite materials are considered. These criteria are nonlinear in nature and involve interactions between the multiaxial stress components. The gust response is based on random gust analysis using state-space mathematical models and statistical properties of gusts in the atmosphere. The covariance matrix of the stress components at a point is used to define a quadratic surface representing stress combinations of equal probability. It is shown how a single critical stress combination can be determined analytically for all stress combinations on the equal-probability stress surface. Analytic sensitivities of the resulting stress constraint with respect to design variables are derived. A constraint function approximation is also derived to reduce computational effort in an approximation–concepts-based optimization strategy. The constraint, analytic sensitivities, and approximations are then integrated into a multidisciplinary aeroservoelastic optimization capability, and results for a large flexible commercial transport airplane are presented.

Nomenclature

$[A]$	=	matrix with terms a_{ij}
$\{b\}, c$	=	coefficients determining the constraint function in normalized coordinates
$[C]$	=	covariance matrix of the gust stress components due to a design gust velocity U_σ
$[C_1]$	=	covariance matrix of the gust stress components due to a unit design gust velocity
$[C(p)]$	=	covariance matrix variation with a design variable p
$[F], \{f\}$	=	matrix and vector defining the quadratic failure criterion
g	=	constraint function
$\bar{g}$	=	constraint function used to determine the critical stress vector
$h()$	=	function value
$[I]$	=	identity matrix
L	=	Lagrangian
N_k	=	total number of design variables
p	=	design variable
p_k	=	kth design variable
$p()$	=	probability density function
$\{q\}$	=	vector of normalized coordinates
s_{xx}, s_{yy}, s_{xy}	=	stress components
$\{s\}$	=	stress vector
$\{s_g\}$	=	stresses due to gust
$\{s_1\}$	=	mean stresses
U_σ	=	design gust velocity
Δ	=	small positive coefficient
Δg	=	correction of the constraint function g to improve the approximation
γ	=	eigenvalue from the eigenvalue problem (10)
γ_j	=	jth eigenvalue
$\gamma_{\max}$	=	maximum eigenvalue
$[\Lambda]$	=	diagonal matrix with eigenvalues along the diagonal
λ	=	Lagrange multiplier
σ_{allow}	=	allowable von Mises stress
$\{\varphi\}$	=	eigenvector from the eigenvalue problem (10)
$[\varphi]$	=	matrix of eigenvectors

Subscripts

i, j	=	ith or jth term in a vector
ij	=	the ith row and jth column in a matrix
max	=	maximum eigenvalue
o	=	reference configuration

Sensitivity of Matrices and Vectors

$\left[\frac{\partial C}{\partial p}\right]$	=	sensitivity of the covariance matrix $[C]$ to changes in the design variable p
$\left\{\frac{\partial s}{\partial p}\right\}$	=	sensitivity of the stress vector $\{s\}$ to changes in the design variable p
$\frac{\partial \gamma_i}{\partial p}$	=	ith diagonal term in $\left[\frac{\partial \Lambda}{\partial p}\right]$
$\left[\frac{\partial \Lambda}{\partial p}\right]$	=	diagonal matrix of eigenvalue sensitivities

Matrices and Vectors

$[\,]$	=	matrix
$\{\,\}$	=	column vector
$\lfloor\,\rfloor$	=	row vector
$[\,]^{-1}$	=	inverse of matrix
$\|\|$	=	determinant of matrix, absolute value of a scalar

Received 26 February 2001; revision received 22 April 2003; accepted for publication 1 July 2003.

*Associate Technical Fellow, Loads and Dynamics; frode.engelsen@boeing.com.

†Professor, Department of Aeronautics and Astronautics; eli@aa.washington.edu. Associate Fellow AIAA.

Introduction

POWER spectral density (PSD) techniques have been applied in the design of airplane structures for many years[1–8] to ensure safe flight through turbulence. The drive to include gust response in integrated control/structure aeroservoelastic synthesis of actively controlled airplanes motivated development of PSD response sensitivity equations[9] as well as alternative state-space analysis and sensitivity techniques.[10–16] The state-space formulation becomes attractive when methods of modern control system modeling and design are used for aeroservoelastic synthesis. Structural failure, due to combined steady-state (maneuver) and gust stresses, is evaluated by considering the probability of exceedance of a stress failure criterion. Whereas the response evaluation is based on the analysis of linear models, important stress failure criteria are nonlinear in nature. Examples include the von Mises and the Tsai–Wu quadratic criteria for isotropic and composite structures,[17,18] respectively.

In the case of multiaxial stress states, such as the two-dimensional plane-stress states in thin structural elements (for example, wing skins), the stress components are statistically correlated and the possibility of failure must be evaluated for all equal-probability combinations of these stresses. An infinite number of stress combinations (for each point on the structure) have to be evaluated, and the resulting computational effort can be prohibitive.

Some attempts have been made to overcome these problems. In the joint probability technique,[19] the failure criterion was used to define a strength envelope or an allowable stress interaction curve. The volume under the joint probability distribution function between the stress components inside the strength envelope is then the probability that the design is safe. Expressions were derived for the number of exceedances per unit time of the structural interaction boundary.[19,20] Unfortunately, exact solutions exist only for a few special cases, and these methods have been found to be too cumbersome for practical applications.

In the matching condition technique,[21,22] which is aimed at high-aspect-ratio beamlike wings, the interaction between shear and torsion internal loads (rather than stresses at points on the structure) at spanwise wing stations was covered by two-dimensional equal-probability ellipses. Octagons circumscribing the ellipses were created, generating eight design points for the possible critical load combinations. The failure criterion (for each span station) was evaluated at each of these points in the octagon. When more than two components (shear, bending, and torsion, or stress components s_{xx}, s_{yy}, s_{xy}) are considered, the equal-probability surface becomes three-dimensional or multidimensional depending on the number of components considered. The number of corner points increases drastically and the method becomes computationally intensive.

This problem was addressed by evaluating the stress failure criterion for a large number of points over the equal-probability ellipses,[23,24] but then lumping the many resulting values into a single cumulative constraint. The cumulative constraint functions for gust-induced stresses were derived and used in an optimization capability. A two-dimensional stress state was assumed based on two principal stresses, thus leading to a two-dimensional equal-probability ellipse. The stress failure function was evaluated at 40 points on the equal-probability surface for each structural member.

Work reported in Ref. 25 led to a procedure for determining critical combined random loads to ensure maximum structural efficiency. Reference 25 shows that in an efficient design, the limit equal-probability surface would be tangent to the strength interaction surface (which defines stress combinations leading to failure) at one or more points. At these critical points, the gradient vectors of the two surfaces are aligned. An exact method for finding the critical points was not developed, however.

In all the aforementioned methods, the evaluation of stress failure constraints is a major computational challenge. For gradient-based optimization, where gradients of constraints are required, the evaluation of stress constraint sensitivities becomes another challenge. Examination of the literature on aeroelastic and aeroservoelastic optimization of aircraft reveals that, because of the difficulties described, constraints on structural failure due to flight in random turbulence have rarely (if ever) been taken into account in a comprehensive manner.

This paper describes a computationally efficient formulation of gust response failure constraints for multiaxial stress combinations. It is shown that it is possible to find, using an analytical formulation, the single most critical point on the equal-probability stress combinations surface for each point in the structure where stresses are evaluated. Once this point is found, the stress constraint and its derivatives with respect to structural and control design variables can be found analytically in closed form.

The key to success of nonlinear programming in solving large-scale aeroservoelastic optimization problems is the use of approximation concepts.[26,27] Rather than calling for detailed analysis (using large-scale models) whenever new values of objective and constraints are required, the optimization routines use computationally efficient approximate objective and constraint functions. A sequence of approximate optimization problems can, thus, be solved efficiently until convergence is reached. In this paper an approximate constraint function (in addition to the exact function and its sensitivities) is derived and presented.

The present work has been developed for interaction failure criteria involving stresses but applies equally well to strain interaction criteria. Additionally, the derivations are made for stress interactions with three components (plane stress) but can easily be extended to n components. In the example graphs, two components are used for simplicity.

Constraint Formulation

Equal-Probability Stress Surfaces and von Mises and Tsai–Wu Quadratic Failure Criteria

The stress vector $\{s\}$ for thin two-dimensional panels consists of two normal stresses, s_{xx} and s_{yy}, and one shear stress component, s_{xy}. These stresses are linear combinations of the incremental stresses due to gust, $\{s_g\}$, and the mean stresses arising from 1-g (or higher g, if necessary) flight $\{s_1\}$:

$$\{s\} = \{s_g\} + \{s_1\} \tag{1}$$

In a linear random response analysis, the stresses due to zero-mean Gaussian gust inputs are Gaussian too. The joint probability density function of the three gust stress components in a plane-stress element is described by[28]

$$p(\{s_g\}) = 1 \Big/ \left[(2\pi)^{\frac{3}{2}} |C_1|^{\frac{1}{2}}\right] \exp\left[-\tfrac{1}{2}\{s_g\}^T [C_1]^{-1} \{s_g\}\right] \tag{2}$$

where $[C_1]$ is the covariance matrix of the gust stress components due to a unit root-mean-square (rms) input gust velocity and $|C_1|$ is its determinant. For a design failure probability level, the relationship between the stress components is given by an equal-probability surface:

$$\{s_g\}^T [C_1]^{-1} \{s_g\} = U_\sigma^2 \tag{3}$$

where U_σ is the design gust velocity in the design envelope criterion described in publications by the regulatory agencies.[1–3] It takes into account the intensity of the input and the number of standard deviations that the equal-probability hyperellipsoid contains. With a design level covariance matrix defined as $[C] = [C_1]U_\sigma^2$ (due to U_σ gust rms velocity input) the equal-probability surface is of the form

$$\{s_g\}^T [C]^{-1} \{s_g\} = 1 \tag{4}$$

Every point on the surface has an equal probability of occurrence and constitutes a possible design point.

In the case of a quadratic failure criterion for a thin panel (or a layer within a panel), the multiaxial stresses will cause failure when the stress vector represents a point outside a closed quadratic surface:

$$\{s\}^T [F] \{s\} + \{f\}^T \{s\} = 1 \tag{5}$$

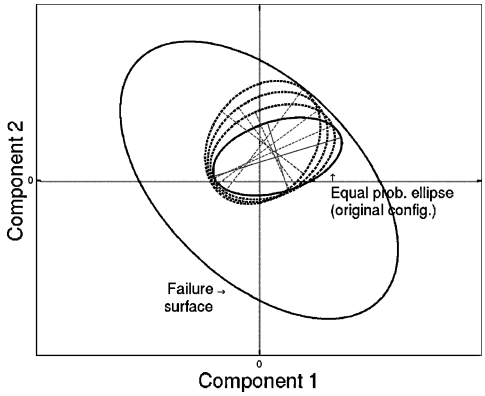

Fig. 1 Equal-probability surface and failure surface for a two-component state of stress. (The equal-probability stress changes with variations in design variables.)

As an example, for an isotropic material the von Mises failure constraint can be written as

$$s_{xx}^2+s_{yy}^2-s_{xx}s_{yy}+3s_{xy}^2=\begin{Bmatrix}s_{xx}\\ s_{yy}\\ s_{xy}\end{Bmatrix}^T\begin{bmatrix}1 & -\frac{1}{2} & 0\\ -\frac{1}{2} & 1 & 0\\ 0 & 0 & 3\end{bmatrix}\begin{Bmatrix}s_{xx}\\ s_{yy}\\ s_{xy}\end{Bmatrix}\le\sigma_{\text{allow}}^2 \tag{6}$$

Equation (6) can be converted to Eq. (5) with the following substitutions:

$$[F]=\frac{1}{\sigma_{\text{allow}}^2}\begin{bmatrix}1 & -\frac{1}{2} & 0\\ -\frac{1}{2} & 1 & 0\\ 0 & 0 & 3\end{bmatrix},\qquad \{f\}=\{0\} \tag{7}$$

For composite materials, the Tsai–Wu failure criterion[17] can also be written in the form of Eq. (5). Figure 1 shows the failure surface and equal-probability stress combination surface for a case involving two stress components. The equal-probability stress ellipse includes stresses due to random gust (zero-mean gust inputs) added to steady stresses due to 1-g flight.

Failure will occur if any point on the equal-probability stress combination surface is outside the failure surface. In other words, failure is prevented if all points on the equal-probability stress surface lie within the failure surface. The stress failure constraint function for design optimization is, therefore,

$$g(s)=\{s\}^T[F]\{s\}+\{f\}^T\{s\}-1\le 0 \tag{8}$$

Most Critical Stress Combination on an Equal-Probability Surface

Instead of evaluating Eq. (8) at an infinite number of points (or a large number of points) on the equal-probability surface, it is sufficient to consider the point $\{s\}$ on the equal-probability surface [Eq. (4)] that will maximize $g(s)$ [Eq. (8)], hence making the constraint most critical. This point is found from a constrained optimization problem as follows: out of all stress combination points on the equal-probability stress hyperellipsoid, find the one that renders the failure criterion, Eq. (8), most critical:

$$\max \bar{g}(s)=\{s\}^T[F]\{s\}+\{f\}^T\{s\}-1$$
$$\text{subject to } (\{s\}-\{s_1\})^T[C]^{-1}(\{s\}-\{s_1\})=1 \tag{9}$$

To simplify the problem a coordinate transformation can be carried out to make both $[C]$ and $[F]$ matrices diagonal simultaneously. Because both matrices are real and symmetric, the eigenvectors $\{\varphi\}$ of the following eigenvalue problem can provide such a transformation:

$$[F]\{s\}=[C]^{-1}\{s\}\gamma \tag{10}$$

The eigenvectors can be placed column by column in an eigenvector matrix $[\varphi]$, and they are normalized so that

$$[\varphi]^T[C]^{-1}[\varphi]=[I] \tag{11}$$

The diagonal matrix $[\Lambda]$ in Eq. (12) contains the eigenvalues. Thus,

$$[\varphi]^T[F][\varphi]=[\Lambda] \tag{12}$$

We can now define

$$\{s\}-\{s_1\}=[\varphi]\{q\}\Rightarrow\{s\}=[\varphi]\{q\}+\{s_1\} \tag{13}$$

The constrained optimization problem can, then, be written as follows:

$$\max \bar{g}(s)=\{q\}^T[\Lambda]\{q\}+\{b\}^T\{q\}+c \tag{14a}$$

subject to

$$\{q\}^T\{q\}=1 \tag{14b}$$

where

$$\{b\}=[\varphi]^T(2[F]\{s_1\}+\{f\}),\qquad c=\{s_1\}^T[F]\{s_1\}+\{f\}^T\{s_1\}-1 \tag{14c}$$

This transformation moves the center of the equal-probability surface to the origin. The axes are scaled such that the equal-probability surface becomes a sphere (or a circle in the two-dimensional case) and the axes are rotated so that the new coordinate axes align with the principal axes of the failure surface. This is illustrated (for the case of two stress components) in Fig. 2.

The method of Lagrange multipliers can now be applied to solve the equality-constrained optimization problem (14). Define a Lagrange function as

$$L(\{q\},\lambda)=\{q\}^T[\Lambda]\{q\}+\{b\}^T\{q\}+c-\lambda(\{q\}^T\{q\}-1) \tag{15}$$

Differentiation with respect to the transformed stress vector $\{q\}$ and Lagrange multiplier λ leads to

$$([\Lambda]-\lambda[I])\{q\}=-\tfrac{1}{2}\{b\},\qquad \{q\}^T\{q\}=1 \tag{16}$$

Solution of the Maximization Problem for the Special Case $\{b\}=\{0\}$

For the special case $\{b\}=\{0\}$, λ must equal one of the eigenvalues, γ_j. Only the jth term of the solution vector $\{q\}$ will then have a nonzero entry, either $+1$ or -1. The value of the objective function will be $\bar{g}=\gamma_j+c$. It is obvious that maximum $\bar{g}$ is obtained when λ equals the largest eigenvalue of Eqs. (10–12).

Figure 3 shows the possible critical points, again for a case with two stress components. In a design optimization case the failure surface for a given material is fixed while the equal-probability stress ellipsoid changes location, size, and orientation because changes in

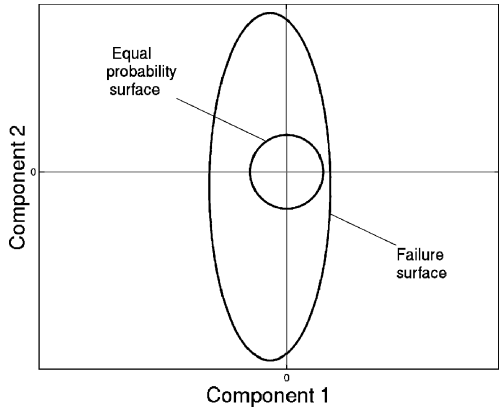

Fig. 2 Equal-probability surface and failure surface in transformed principal coordinates.

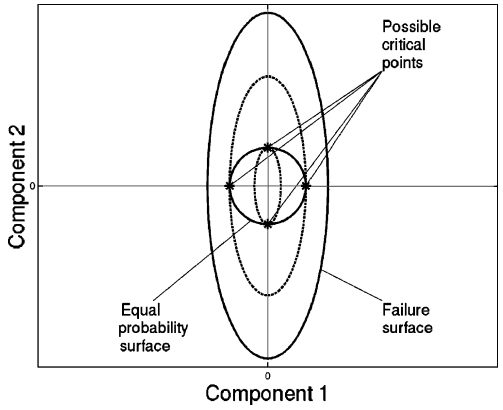

Fig. 3 Possible critical points using principal coordinates (two-component case, the special case $\{b\} = \{0\}$).

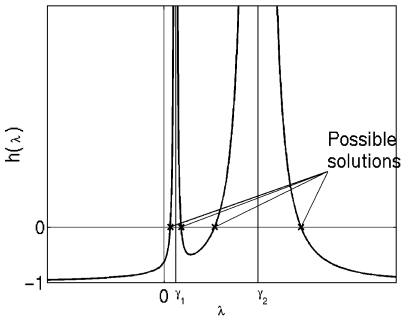

Fig. 4 Left-hand side of Eq. (18) used to determine the Lagrange multiplier λ.

the design lead to changes of resulting stresses. For the purpose of illustration, the failure function generates ellipses (dashed lines) that are varied in Fig. 3 to show possible points of contact between the two surfaces. Increased values of $\bar{g}$ represent larger ellipses. At the critical points, the gradient vector of the failure surface aligns with the gradient vector of the circle (equal-probability surface). In this special case, all curves are centered at the origin. There are two eigenvalues and four possible critical points at opposite ends of the principal axes of the ellipses. The vector $\{\boldsymbol{q}\}$ determines the locations of the critical points. Because the length of a principal axis is $1/\gamma$, the smallest principal axis corresponds to the largest eigenvalue, and it is clear from the figure why this also results in the largest value of $\bar{g}$.

Solution of the Maximization Problem in the General Nonzero $\{b\}$ Case

In the general case, when $\{\boldsymbol{b}\}$ is nonzero,

$$\{\boldsymbol{q}\} = -\tfrac{1}{2}([\Lambda] - \lambda[I])^{-1}\{b\} \Rightarrow \boldsymbol{q}_i = -\tfrac{1}{2}b_i/(\gamma_i - \lambda) \qquad (17)$$

This solution must satisfy the constraint equation $\{\boldsymbol{q}\}^T\{\boldsymbol{q}\} = 1$.

$$\frac{1}{4}\{b\}^T([\Lambda] - \lambda[I])^{-2}\{b\} = 1 \Rightarrow h(\lambda) = \sum_i \frac{1}{4}\frac{b_i^2}{(\gamma_i - \lambda)^2} - 1 = 0 \qquad (18)$$

The Lagrange multiplier λ can be found from Eq. (18). With n stress components the order of the equation becomes $2n$ with $2n$ possible solutions. A typical graph of $h(\lambda)$ for two stress components is shown in Fig. 4.

The function value h will approach -1 for large positive or negative values of λ and approach infinity when λ approaches any of the eigenvalues. From the figure it can be seen that there will be one possible solution on each side of the eigenvalues. Among the possible solutions, the solution resulting in highest $\bar{g}$ is sought.

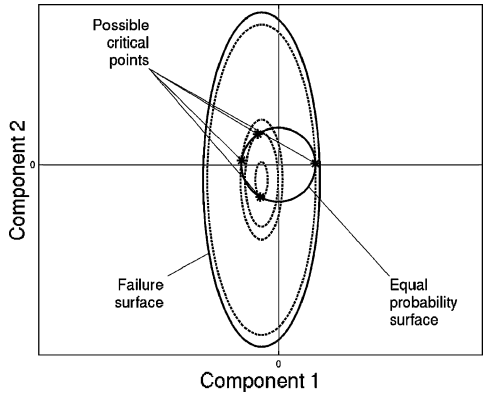

Fig. 5 Possible solutions of the critical point constraint maximization problem.

With the expression for $\{\boldsymbol{q}\}$ in Eq. (17), the extreme value of $\bar{g}$ becomes

$$\bar{g}(s) = c + \sum_i \frac{1}{4}\frac{b_i^2}{(\gamma_i - \lambda)^2}(2\lambda - \gamma_i) \qquad (19)$$

The Lagrange multiplier λ has to satisfy Eq. (18). Each of the terms $\frac{1}{4}b_i^2/(\gamma_i - \lambda)^2$ is positive and their sum equals 1. It is clear [considering Eq. (18)] that because each of the $\frac{1}{4}b_i^2/(\gamma_i - \lambda)^2$ terms in Eq. (19) is multiplied by a factor of $2\lambda - \gamma_i$, the value of the sum in Eq. (19) will be a maximum when those factors are largest, corresponding to the largest Lagrange multiplier that renders all those factors positive. Because there exist two potential solutions close to each of the eigenvalues γ_i, $\lambda = \gamma_i \pm \Delta$, one of the terms $\frac{1}{4}[b_i^2/(\gamma_i - \lambda)^2] = \frac{1}{4}(b_i^2/\Delta^2)$ becomes much larger than the others and will be close to 1. The maximum constraint function value is therefore dominated by the term

$$\bar{g}(s) \approx c + \tfrac{1}{4}\left[b_i^2\big/(\gamma_i - \lambda)^2\right](2\lambda - \gamma_i) \approx c + \tfrac{1}{4}\left(b_i^2\big/\Delta^2\right)(\gamma_i \pm 2\Delta)$$
$$\approx c + (\gamma_i \pm 2\Delta) \qquad (20)$$

From Eq. (20) it can be seen that the largest value of the constraint function can be obtained when λ is slightly higher than the highest eigenvalue. Therefore, it is only necessary to determine this value of λ. This agrees with the results obtained in the special case where $\{b\} = \{0\}$.

Figure 5 shows an example for two stress components. As the failure surface is shrunk toward the equal-probability stress surface, four possible critical points are indicated. (Alternatively the equal-probability stress surface could be increased in size toward a given failure surface.)

The sought value of λ can be found by an iterative Newton–Raphson method applied to Eq. (18). The iterative scheme uses

$$\lambda_{j+1} = \lambda_j - \frac{h(\lambda_j)}{\mathrm{d}h/\mathrm{d}\lambda(\lambda_j)} \qquad (21)$$

where

$$h(\lambda_j) = -1 + \sum_i \frac{1}{4}\frac{b_i^2}{(\gamma_i - \lambda_j)^2}, \qquad \frac{\mathrm{d}h}{\mathrm{d}\lambda}(\lambda_j) = \sum_i \frac{1}{2}\frac{b_i^2}{(\gamma_i - \lambda_j)^3} \qquad (22)$$

The iteration starts with a value of λ_j slightly larger than the highest eigenvalue. Under the assumption that

$$\tfrac{1}{4}\left[b_i^2\big/(\gamma_{\max} - \lambda)^2\right] \approx 1$$

a starting value is

$$\lambda_0 = \gamma_{\max} + |b_i|/2 \qquad (23)$$

With this starting value, the solution converges within a couple of iterations. Expression (23) can also be used as an approximate value for λ when an iterative scheme is not desired.

Analytical Sensitivity Derivation

The sensitivity of the stresses with respect to a design variable p can be attributed to changes in the gust covariance matrix $[\partial C/\partial p]$ as well as the sensitivity of the steady 1-g mean stresses $\{\partial s_1/\partial p\}$. The sensitivity of the constraint function (14) is

$$\frac{\partial g}{\partial p} = \frac{\partial \bar{g}}{\partial p} = (2\{\boldsymbol{q}\}^T[\Lambda] + \{b\}^T)\left\{\frac{\partial q}{\partial p}\right\} + \{\boldsymbol{q}\}^T\left[\frac{\partial \Lambda}{\partial p}\right]\{\boldsymbol{q}\} + \left\{\frac{\partial b}{\partial p}\right\}^T\{\boldsymbol{q}\} + \frac{\partial c}{\partial p} \tag{24}$$

where

$$\left\{\frac{\partial b}{\partial p}\right\} = \left[\frac{\partial \varphi}{\partial p}\right]^T(2[F]\{s_1\} + \{\boldsymbol{f}\}) + 2[\varphi]^T[F]\left\{\frac{\partial s_1}{\partial p}\right\}$$

$$\frac{\partial c}{\partial p} = 2\{s_1\}[F]\left\{\frac{\partial s_1}{\partial p}\right\} + \{\boldsymbol{f}\}^T\left\{\frac{\partial s_1}{\partial p}\right\} \tag{25}$$

Because all of the eigenvectors are known and the eigenvalues are distinct, the eigenvector sensitivities can be written as a linear superposition of the eigenvectors[29]:

$$\left[\frac{\partial \varphi}{\partial p}\right] = [\varphi][A] \tag{26}$$

The eigenvectors and eigenvalues satisfy the equation

$$[C][F][\varphi] = [\varphi][\Lambda] \tag{27}$$

Taking the derivative of Eq. (27) with respect to design variable p and utilizing Eq. (26),

$$\left[\frac{\partial C}{\partial p}\right][F][\varphi] + [C][F][\varphi][A] = [\varphi][A][\Lambda] + [\varphi]\left[\frac{\partial \Lambda}{\partial p}\right] \tag{28}$$

By premultiplying Eq. (28) by $[\varphi]^T[F]$ and utilizing definitions (12) and (27), we get

$$[\varphi]^T[F]\left[\frac{\partial C}{\partial p}\right][F][\varphi] + [\Lambda][\Lambda][A] = [\Lambda][A][\Lambda] + [\Lambda]\left[\frac{\partial \Lambda}{\partial p}\right] \tag{29}$$

Differentiation of Eq. (12) with respect to design variable p and utilization of Eq. (26) leads to

$$\left[\frac{\partial \Lambda}{\partial p}\right] = [A]^T[\Lambda] + [\Lambda][A] \tag{30}$$

Equation (30) is now inserted into Eq. (29) to yield

$$[\varphi]^T[F]\left[\frac{\partial C}{\partial p}\right][F][\varphi] = [\Lambda][A][\Lambda] + [\Lambda][A]^T[\Lambda] \tag{31}$$

With a_{ij} denoting the ijth term in the matrix $[A]$ and $\partial\gamma_i/\partial p$ the ith diagonal term in $[\partial\Lambda/\partial p]$, the diagonal terms of Eqs. (29) and (31) result in the following expressions:

$$a_{ii} = \frac{1}{2}\frac{1}{\gamma_i^2}\{\varphi_i\}^T[F]\left[\frac{\partial C}{\partial p}\right][F]\{\varphi_i\} \qquad \text{for} \qquad i = j \tag{32}$$

$$\frac{\partial \gamma_i}{\partial p} = \frac{1}{\gamma_i}\{\varphi_i\}^T[F]\left[\frac{\partial C}{\partial p}\right][F]\{\varphi_i\} \tag{33}$$

and since the matrices $[\Lambda]$ and $[\partial\Lambda/\partial p]$ are diagonal, the off-diagonal terms in $[A]$ can be obtained from Eq. (29):

$$a_{ij} = \frac{1}{\gamma_i(\gamma_j - \gamma_i)}\{\varphi_i\}^T[F]\left[\frac{\partial C}{\partial p}\right][F]\{\varphi_j\} \qquad \text{for} \qquad i \neq j \tag{34}$$

We can now proceed to evaluate the sensitivities of the extremal $\{\boldsymbol{q}\}$ and λ value leading to the critical constraint value. Equation (16) is differentiated with respect to the design variable p:

$$\left(\left[\frac{\partial \Lambda}{\partial p}\right] - \frac{\partial \lambda}{\partial p}[I]\right)\{\boldsymbol{q}\} + ([\Lambda] - \lambda[I])\left\{\frac{\partial q}{\partial p}\right\} = -\frac{1}{2}\left\{\frac{\partial b}{\partial p}\right\}$$

$$\{\boldsymbol{q}\}^T\left\{\frac{\partial q}{\partial p}\right\} = 0 \tag{35}$$

Equations (35) are combined to yield

$$\frac{\partial \lambda}{\partial p} = \frac{\{\boldsymbol{q}\}^T([\Lambda] - \lambda[I])^{-1}\left(\frac{1}{2}\{\partial b/\partial p\} + [\partial\Lambda/\partial p]\{\boldsymbol{q}\}\right)}{\{\boldsymbol{q}\}^T([\Lambda] - \lambda[I])^{-1}\{\boldsymbol{q}\}} \tag{36}$$

$$\left\{\frac{\partial q}{\partial p}\right\} = -([\Lambda] - \lambda[I])^{-1}\left(\frac{1}{2}\left\{\frac{\partial b}{\partial p}\right\} + \left(\left[\frac{\partial \Lambda}{\partial p}\right] - \frac{\partial \lambda}{\partial p}[I]\right)\{\boldsymbol{q}\}\right) \tag{37}$$

In the special case when $\{b\} = \{0\}$, Eq. (35) is of the form

$$\left(\frac{\mathrm{d}\gamma_i}{\mathrm{d}p} - \frac{\mathrm{d}\lambda}{\mathrm{d}p}\right)q_i + (\gamma_i - \lambda)\frac{\mathrm{d}q_i}{\mathrm{d}p} = 0, \qquad i = 1, 2, \ldots$$

$$\sum_i q_i \frac{\partial q_i}{\partial p} = 0 \tag{38}$$

If $\lambda = \gamma_j$, then

$$q_i = \begin{cases} 0, & i \neq j \\ \pm 1, & i = j \end{cases}$$

and it can be deduced from Eq. (38) that

$$\left\{\frac{\mathrm{d}q}{\mathrm{d}p}\right\} = \{0\}$$

Approximations

The key to the success of nonlinear programming in solving optimization problems is the use of approximation concepts. These are aimed at reducing the number of detailed analyses needed during the optimization and, thereby, reducing the computational cost. In each stage of the optimization process, a detailed analysis and the associated behavior sensitivity analysis are used for constructing approximations of the objective and constraint functions in terms of the design variables. The optimization routines use only these approximate objective and constraint functions. A sequence of approximate optimization problems is carried out until convergence is reached.

Direct and reciprocal Taylor-series approximations[30,31] may capture the constraint function variations in many cases. However, in airplane configurations with lightly damped structural modes, as design variations lead to reduction in damping in some aeroservoelastic poles, large nonlinear variations in the gust stress covariance matrix may be present, and these, in turn, will lead to large variations of the stress failure constraint function. The approach here is to augment the linear approximation by adding a correction term to capture this nonlinear behavior. When a Taylor series in the direct design variables is used,

$$\bar{g}(p) = \bar{g}_o + \sum_{k=1}^{N_k}\left[\left(\frac{\overline{\partial g}}{\partial p_k}\right)_o (p_k - p_{ko}) + \Delta g(p_k)\right] \tag{39}$$

The summation is taken over N_k design variables and the subscript o denotes the reference configuration results available from detailed analysis. The linear portion of the approximation can of course be replaced by a reciprocal approximation.

The correction term Δg is derived as follows: By assuming that the term associated with the maximum eigenvalue is dominant in

expression (19), and by using the value of the Lagrange multiplier defined in Eq. (23), an approximate constraint function expression is

$$\bar{g} = c + \gamma_{\max} + |b_{\max}| \tag{40}$$

where

$$b_{\max} = \{\varphi_{\max}\}^T (2[F]\{s_1\} + \{f\})$$

$$c = \{s_1\}^T [F]\{s_1\} + \{f\}^T \{s_1\} - 1 \tag{41}$$

The subscript max indicates the term associated with the maximum eigenvalue. By inspecting Eqs. (40) and (41) it is apparent that the nonlinear behavior of the constraint function is due to large variations of the maximum eigenvalue $\gamma_{\max}$. Even though the eigenvalues of the small eigenvalue problem (10) can be calculated without significant computational cost, it is attractive to use an approximate expression, a Rayleigh quotient approximation, for example:

$$\gamma_{\max}(p) = \frac{\{\varphi_{\max}\}_o^T [C(p)][F]\{\varphi_{\max}\}_o}{\{\varphi_{\max}\}_o^T \{\varphi_{\max}\}_o} \tag{42}$$

This expression is derived from the eigenvalue problem in expression (10) assuming that the eigenvector does not change from the reference value. A large nonlinear variation of the stress covariance matrix $[C(p)]$ will result in a large variation of the maximum eigenvalue. An accurate approximation of the covariance matrix, capable of capturing its behavior as aeroservoelastic poles lose damping with design variations, is necessary here. The method described in Ref. 16 is one such approximation.

The correction term in Eq. (39) can therefore be written in the form

$$\Delta g(p_k) = \gamma_{\max}(p_k) - \gamma_{\max}(p_{ko}) - \left(\frac{\partial \gamma_{\max}}{\partial p_k}\right)_o (p_k - p_{ko}) \tag{43}$$

where

$$\left(\frac{\gamma_{\max}}{\partial p_k}\right)_o = \frac{\{\varphi_{\max}\}_o^T [\partial C/\partial p_k]_o [F]\{\varphi_{\max}\}_o}{\{\varphi_{\max}\}_o^T \{\varphi_{\max}\}_o} \tag{44}$$

and Eq. (42) are used in Eq. (43).

The correction term vanishes as the maximum eigenvalue varies linearly with changes in the design variables.

Application

The new methodology just described has been implemented in an efficient, integrated aeroservoelastic design optimization capability, the Lifting Surface Control Augmented Structural Synthesis (LS-CLASS) code,[30,32] and has been applied to a typical large, flexible commercial transport configuration. The structural model is based on an equivalent-plate formulation[33–36] for wing, controls, and tail surfaces, and is integrated with doublet lattice unsteady aerodynamics in the Elfini code.[37]

The equivalent-plate model is shown in Fig. 6. The model consists of plate zones (same Ritz displacement functions on a zone) joined with lumped springs. Spars, stringers, ribs, and skins are included in the model. Rigid plate elements are used to model engines, while the fuselage is modeled as a chain of plate/beam segments connected by proper springs.

The aerodynamic mesh is presented in Fig. 7. The wings, engines, horizontal stabilizers, and vertical fin are incorporated into the unsteady calculations. The fuselage aerodynamic distribution is introduced by scaling rigid airplane empirical distribution based on the local deformation along the fuselage centerline. There are no interference effects between the fuselage and the remaining aerodynamic surfaces.

The unsteady generalized aerodynamic forces, calculated at discrete reduced frequencies, are approximated in terms of rational functions of the Laplace variable. Roger's method[38] is used.

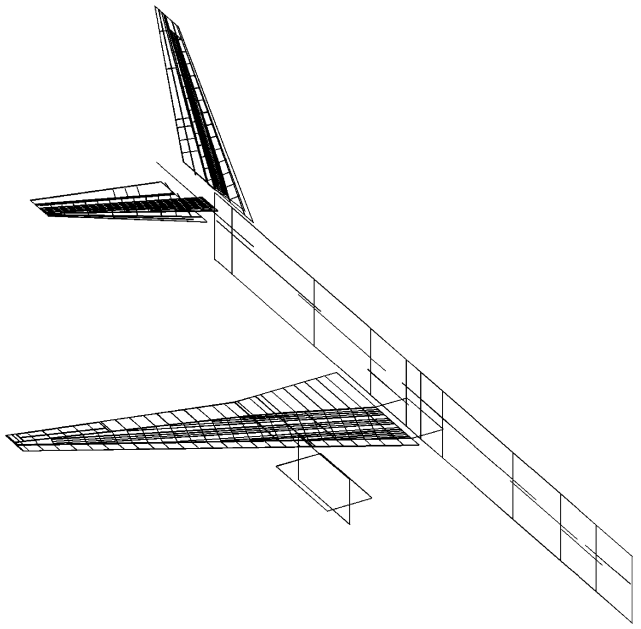

Fig. 6 Equivalent plate structural model of a passenger airplane configuration (plate segments and spar segments shown).

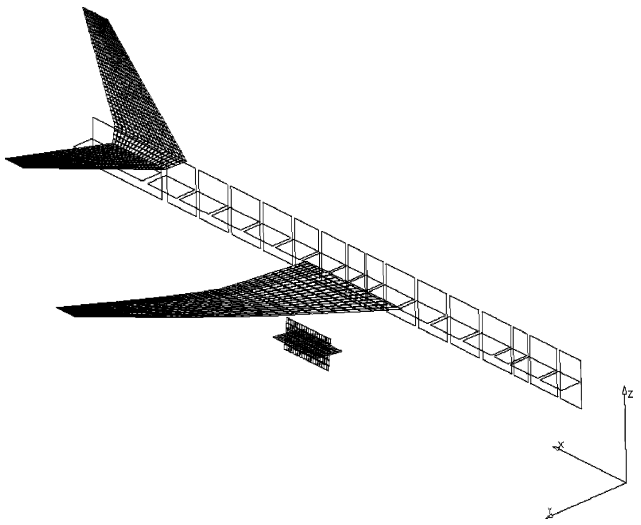

Fig. 7 Doublet lattice aerodynamic mesh for the passenger airplane configuration.

State-space formulations of the control system, actuator dynamics, and sensor dynamics are derived based on transfer function descriptions for sensors, control laws, and actuators (Fig. 8) and combined with the airplane dynamic aeroelastic model.[14,30]

The integrated aeroservoelastic system is modeled as a linear time-invariant (LTI) system. A rational approximation to the von Karman spectrum[39] is used to transform a Gaussian zero-mean white noise input into the gust velocity. The resulting LTI system therefore represents the state-space response due to white noise input. The state covariance matrix is a solution of a Lyapunov matrix equation.[28] The covariance of the stress components can be determined from the state covariance matrix. The stresses due to 1-g level flight, obtained from a static aeroelastic maneuver solution,[14,30] are also taken into account. Accuracy of analysis results of the aeroservoelastic LS-CLASS model was checked against results obtained for the airplane using standard industry analysis tools and was found to be good.[40]

In the multidisciplinary analysis capability, structural design variables (skin thicknesses, spar and stringer cap areas, spring stiffnesses, etc.) and control system design variables (coefficients of

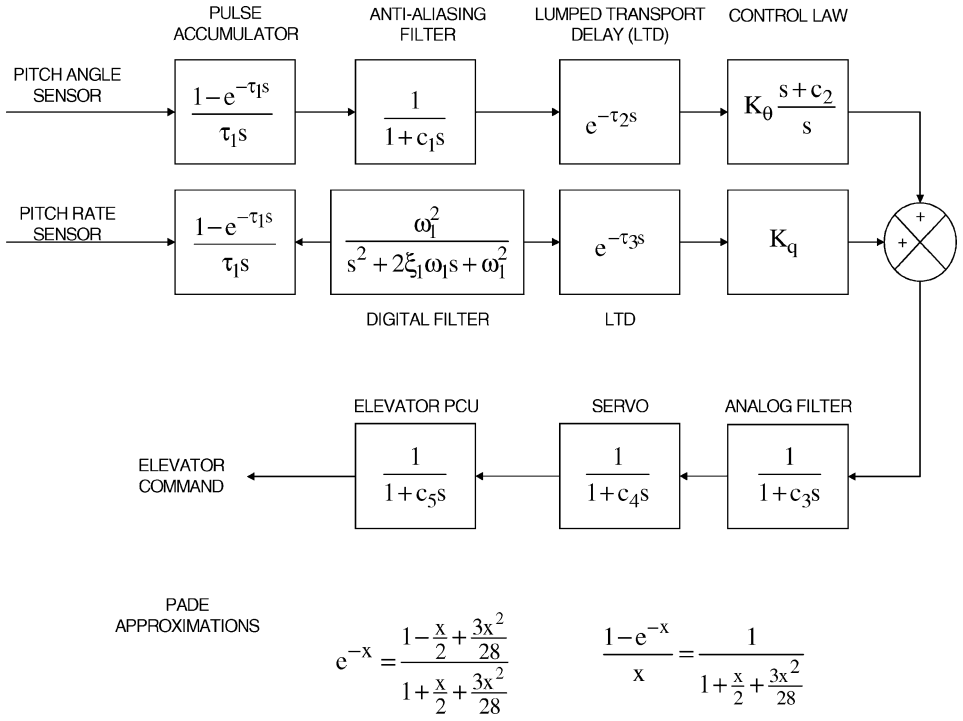

Fig. 8 Control system.

control law transfer functions) can be considered. The sensitivities of the stress covariance matrices due to changes in the design variables can also be found from a Lyapunov matrix equation.[13–15,30]

Results

For a flight condition with design gust velocity $U_\sigma = 85$ fps (25.91 m/s), the stress covariance matrix and 1-g stress vector for a point on the skin of the inboard wing are shown as follows:

$$[C] = \begin{bmatrix} 29{,}493^2 & 0.950 * 29{,}493 * 23{,}058 & -0.919 * 29{,}493 * 5729 \\ \vdots & 23{,}058^2 & -0.976 * 23{,}058 * 5729 \\ \text{symmetric} & \cdots & 5729^2 \end{bmatrix} (\text{psi}^2)$$

$$\{s_1\} = \begin{Bmatrix} -30{,}596 \\ -21{,}944 \\ 2860 \end{Bmatrix} (\text{psi})$$

or

$$[C] = \begin{bmatrix} 2.0338^2 & 0.950 * 2.0338 * 1.5901 & -0.919 * 2.0338 * 0.3951 \\ \vdots & 1.5901^2 & -0.976 * 1.5901 * 0.3951 \\ \text{symmetric} & \cdots & 0.3951^2 \end{bmatrix} \times 10^{16} (\text{N/m}^2)$$

$$\{s_1\} = \begin{Bmatrix} -2.11 \\ -1.51 \\ 0.20 \end{Bmatrix} \times 10^8 (\text{N/m}^2)$$

The diagonal terms of the covariance matrix represent the square of the design level of each stress component due to the gust excitation alone. Because the wing has aluminum cover skins, a von Mises criterion [Eq. (7)] is applied with an allowable stress $\sigma_{\text{allow}} = 60{,}000$ psi (4.1376×10^8 N/m^2).

With these values, the constraint function [Eq. (8)] will have a value of $g = -0.136$. A negative value indicates a safe design. The critical stress point on the equal-probability stress ellipsoid (that is, the stress combination closest to the failure surface) is

$$\lfloor s_{xx} \quad s_{yy} \quad s_{xy} \rfloor_{\text{critical}} = \lfloor -59{,}946 \quad -44{,}433 \quad 8307 \rfloor \text{psi}$$

$$= \lfloor -4.1340 \quad -3.0641 \quad 0.5728 \rfloor \times 10^8 \text{ N/m}^2$$

To validate the analytical sensitivities just derived, the variation in the constraint function with changes in an outboard wing rear spar cap area is presented in Fig. 9. A linear extrapolation using the analytical sensitivity is also presented. The linear curve based on the calculated analytic sensitivity is tangent to the "exact" parametric curve at the baseline configuration (design variable ratio = 1), indicating that the sensitivity calculations are valid. It is clear from Fig. 9 that the linear approximation can capture changes in the constraint function over a wide range of changes in the design variable in this particular case. In airplane configurations with lightly damped structural modes, however, large nonlinear variations in the gust

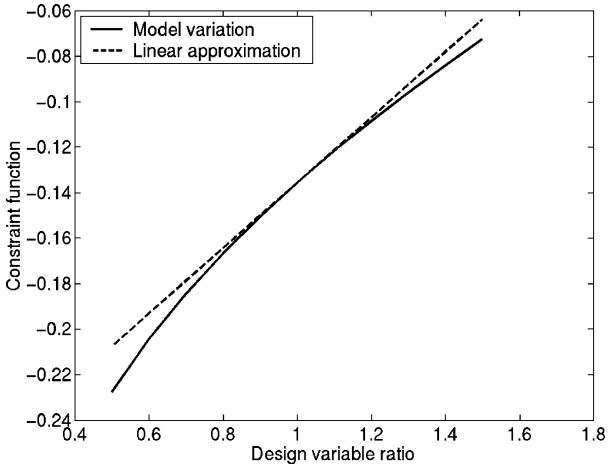

Fig. 9 Stress failure constraint function variation based on a spar cap area design variable change.

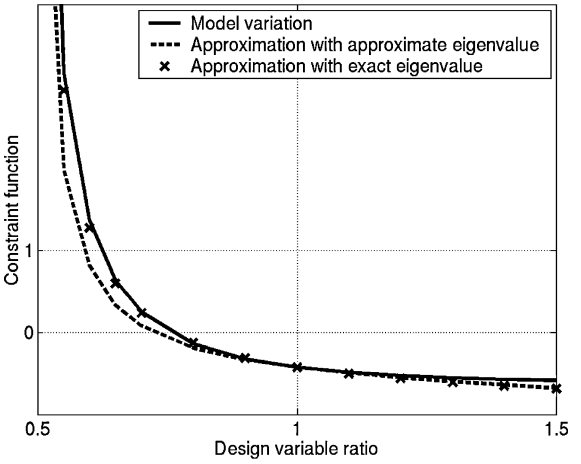

Fig. 11 Stress failure constraint function approximations as a function of spar cap area design variable variations using exact and approximate eigenvalues.

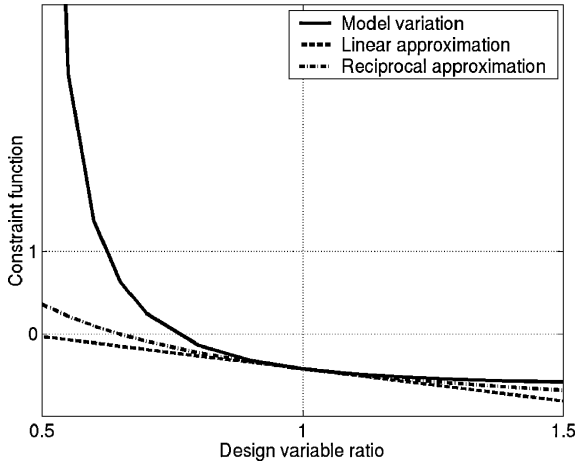

Fig. 10 Linear and reciprocal Taylor-series approximations of a stress failure constraint function in the case of a lightly damped aeroelastic system. Effects of variations of a spar cap area design variable are shown.

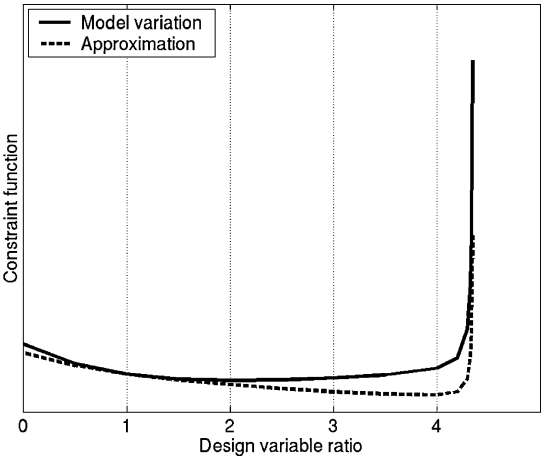

Fig. 12 Stress failure constraint function approximation for a control system gain design variable.

stress covariance matrix and the constraint functions may occur[16] when changes in design variables push the system toward instability. As the damping in any aeroservoelastic pole is reduced toward zero damping and subsequent instability, the covariance response shoots to infinity. From Fig. 10 it is clear that Taylor-series-based linear or reciprocal approximation techniques[27,31] cannot capture such variations accurately.

Figure 11 shows the performance of the new constraint approximation [Eq. (39)] derived here using both exact and approximate expressions for the maximum eigenvalue. Both approximations capture the rise in the constraint function well. With an exact eigenvalue (obtained at a very small computational cost from the solution of a three-dimensional eigenvalue problem), the approximation is almost perfect. This indicates that the assumption of one dominant term in Eq. (19) is good and that improved accuracy may be obtained by improving the quality of the eigenvalue approximation, for example, by accounting for eigenvector sensitivities. The approximation based on an approximate maximum eigenvalue also captures the nonlinear behavior, although the rise in response toward infinity is at slightly different design variable values. It is very computationally efficient.

The approximation is also shown for a variation of a control system gain in Fig. 12. The approximation is valid over a wide range of changes in the design variable and captures the location of the rise. This does, however, assume that the rise is reflected in the stress covariance matrix. Approximations of this matrix are discussed in Ref. 16 and are the subject of a new paper.[41]

Conclusions

Computationally efficient gust stress constraints for multiaxial stress combinations have been derived. Unlike previous methods, the new constraint function is based on the identification of a single critical stress combination point and, thus, overcomes the difficulty presented by the need to cover all stress combinations on the equal-probability stress surface. Analytical sensitivities due to changes in design variables (both structural and control system design variables) are also derived. An efficient approximation that can capture nonlinear variations in gust response over a wide range of design variables is derived. The new formulations have been implemented in an efficient integrated aeroservoelastic optimization capability, and results have been shown for a typical large commercial transport airplane configuration. It is through their effects on dynamic stresses due to flight in turbulence, among other constraints, that active control and structural design variables interact on actively controlled optimized flight vehicles. The development presented in this paper is aimed at introducing gust stress failure criteria into the framework of integrated control/structure aeroservoelastic synthesis.

References

[1]"Continuous Gust Design Criteria," *Federal Aviation Regulations, Part 25*, App. G, Federal Aviation Administration, Dept. of Transportation, 1998, App. G.

[2]"Joint Aviation Requirements, JAR-25," Joint Aviation Authorities, ACJ 25.341(b), Hoofddorp, The Netherlands, 1994.

[3]Hoblit, F. M., *Gust Loads on Aircraft: Concepts and Applications*, AIAA, Washington DC, 1988.

[4]Houbolt, J. C., Steiner, R., and Pratt, K. G., "Dynamic Response of Airplanes to Atmospheric Turbulence Including Flight Data on Input and Response," NASA TR-R-199, 1964.

[5]Mitchell, C. G. B., "Assessment of the Accuracy of Gust Response Calculations by Comparison with Experiments," *Journal of Aircraft*, Vol. 7, No. 2, 1970, pp. 117–125.

[6]Perry, B., III, Kroll, R. I., Miller, R. D., and Goetz, R. C., "DYLOFLEX: A Computer Program for Flexible Aircraft Flight Dynamic Loads Analysis with Active Controls," *Journal of Aircraft*, Vol. 17, No. 4, 1980, pp. 275–282.

[7]"Handbook for Aeroelastic Analysis," MSC/NASTRAN Version 65, The MacNeal-Schwendler Corp., Los Angeles, 1987.

[8]Crimaldi, J. P., Britt, R. T., and Rodden, W. P., "Response of the USAF/NORTHROP B-2 Aircraft to Nonuniform Spanwise Atmospheric Turbulence," *Proceedings of the AIAA/ASME/ASCE/ASC/AHS Structures, Structural Dynamics, and Materials Conference*, AIAA, Washington, DC, 1991, pp. 1728–1741.

[9]D'vari, R., and Baker, M., "Aeroelastic Loads and Sensitivity Analysis for Structural Loads Optimization," *Journal of Aircraft*, Vol. 36, No. 1, 1999, pp. 156–166.

[10]Gangsaas, D., and Ly, U.-L., "Application of a Modified Linear Quadratic Gaussian Design to Active Control of a Transport Airplane," AIAA Paper 79-1746, Aug. 1979.

[11]Gangsaas, D., Ly, U.-L., and Norman, D. C., "Practical Gust Load Alleviation and Flutter Suppression Control Laws Based on a LQG Methodology," AIAA Paper 81-0021, Jan. 1981.

[12]Lind, R., and Brenner, M., *Robust Aeroservoelastic Stability Analysis*, Springer-Verlag, London, 1999.

[13]Mukhopadhyay, V., Newsom, J. R., and Abel, I., "A Method for Obtaining Reduced-Order Control Laws for High-Order Systems Using Optimization Techniques," NASA TP-1876, 1981.

[14]Livne, E., Schmit, L. A., and Friedmann, P. P., "Towards an Integrated Approach to the Optimum Design of Actively Controlled Composite Wings," *Journal of Aircraft*, Vol. 27, No. 12, 1990, pp. 979–992.

[15]Zole, A., and Karpel, M., "Continuous Gust Response and Sensitivity Derivatives Using State-Space Models," *Journal of Aircraft*, Vol. 31, No. 5, 1994, pp. 1212–1214.

[16]Livne, E., "Alternative Approximations for Integrated Control/Structure Aeroservoelastic Synthesis," *AIAA Journal*, Vol. 31, No. 6, 1993, pp. 1100–1108.

[17]Tsai, S. W., and Hahn, H. T., *Introduction to Composite Materials*, Technomic, Westport, CT, 1980, Chap. 7.

[18]Burk, R. C., "Standard Failure Criteria Needed for Advanced Composites," *Astronautics and Aeronautics*, June 1983, pp. 58–62.

[19]Fuller, J. R., Richmond, L. D., Larkins, C. D., and Russel, S. W., "Contributions to the Development of a Power-Spectral Gust Design Procedure for Civil Aircraft," Federal Aviation Agency, TR FAA-ADS-54, Jan. 1966.

[20]Houbolt, J. C., "Exceedances of Structural Interaction Boundaries for Random Excitation," *AIAA Journal*, Vol. 6, No. 11, 1968, pp. 2175–2182.

[21]Hoblit, F. M., Paul, N., Shelton, J. D., and Ashford, F. E., "Development of a Power-Spectral Gust Design Procedure for Civil Aircraft," Federal Aviation Agency, TR FAA-ADS-53, Jan. 1966.

[22]Stauffer, W. A., and Hoblit, F. M., "Dynamic Gust, Landing, and Taxi Loads Determination in the Design of the L-1011," *Journal of Aircraft*, Vol. 10, No. 8, 1973, pp. 459–467.

[23]Hajela, P., and Bach, C. T., "Optimum Structural Sizing for Gust Induced Response," *Proceedings of 29th AIAA/ASME/ASCE/AHS/ASC Structures, Structural Dynamics, and Materials Conference*, AIAA, Washington, DC, 1988, pp. 681–688.

[24]Hajela, P., and Bach, C. T., "Optimum Structural Sizing for Gust-Induced Response," *Journal of Aircraft*, Vol. 26, No. 4, 1989, pp. 395–397.

[25]Fuller, J. R., "Boundary Excursions for Combined Random Loads," *AIAA Journal*, Vol. 20, No. 9, 1982, pp. 1300–1305.

[26]Schmit, L. A., "Structural Optimization—Some Key Ideas and Insights," *New Directions in Optimum Structural Design*, edited by E. Atrek, R. H. Gallagher, K. M. Ragsdell, and O. C. Zienkiewicz, Wiley, New York, 1984.

[27]Haftka, R. T., and Gurdal, Z., *Elements of Structural Optimization*, 3rd rev. and expanded ed., Kluwer Academic, Dorecht, The Netherlands, 1992, Chap. 6.

[28]Bryson, A. E., and Ho, Y.-C., *Applied Optimal Control*, Ginn, Waltham, MA, 1969, Chaps. 10, 11.

[29]Fox, R. L., and Kapoor, M. P., "Rate of Change of Eigenvalues and Eigenvectors, " *AIAA Journal*, Vol. 6, No. 12, 1968, pp. 2426–2429.

[30]Livne, E., "Integrated Multidisciplinary Optimization of Actively Controlled Fiber Composite Wings," Ph.D. Dissertation, Dept. of Mechanical, Aerospace, and Nuclear Engineering, Univ. of California, Los Angeles, 1990.

[31]Livne, E., "Integrated Aeroservoelastic Optimization: Status and Direction," *Journal of Aircraft*, Vol. 36, No. 1, 1999, pp. 122–145.

[32]Livne, E., Schmit, L. A., and Friedmann, P. P., "Integrated Structure/Control/Aerodynamic Synthesis of Actively Controlled Composite Wings," *Journal of Aircraft*, Vol. 30, No. 3, 1993, pp. 387–394.

[33]Livne, E., Schmit, L. A., and Friedman, P., "Design Oriented Structural Analysis for Fiber Composite Wings," Univ. of California, UCLA-ENG-88-35, Los Angeles, Nov. 1988.

[34]Giles, G. L., "Equivalent Plate Modeling for Conceptual Design of Aircraft Wing Structures," AIAA Paper 95-3945, Sept. 1995.

[35]Giles, G. L., "Design Oriented Analysis of Fuselage Structures Using Equivalent Plate Methodology," *Journal of Aircraft*, Vol. 36, No. 1, 1999, pp. 21–28.

[36]Livne, E., Sels, R. A., and Bhatia, K. G., "Lessons from Application of Equivalent Plate Structural Modeling to an HSCT Wing," *Journal of Aircraft*, Vol. 31, No. 4, 1994, pp. 953–960.

[37]Nicot, P., and Petiau, C., "Aeroelastic Analysis Using Finite Element Models," DGLR/AAAF/RAES European Forum on Aeroelasticity and Structural Dynamics, Aachen, Germany, April 1989.

[38]Roger, K. L., "Airplane Math Modeling Methods for Active Control Design," *Structural Aspects of Active Controls*, CP-228, AGARD, Aug. 1977, pp. 4–11.

[39]Campbell, C. W., "Monte Carlo Turbulence Simulation Using Rational Approximations to von Kármán Spectra," *AIAA Journal*, Vol. 24, No. 1, 1986, pp. 62–66.

[40]Engelsen, F., "Design-Oriented Gust Stress Constraints for Aeroservoelastic Design Synthesis," Ph.D. Dissertation, Dept. of Aeronautics and Astronautics, Univ. of Washington, Seattle, WA, Aug. 2001.

[41]Engelsen, F., and Livne, E., "Mode Acceleration Based Random Gust Stresses in Aeroservoelastic Optimization," *Journal of Aircraft* (to be published).

A. M. Baz
Associate Editor